Eur. Phys. J. A **25**, s01, 659–664 (2005)
DOI: 10.1140/epjad/i2005-06-133-x

EPJ A direct
electronic only

Shell-model applications in supernova physics

G. Martínez-Pinedo[a]

ICREA and Institut d'Estudis Espacials de Catalunya, Universitat Autònoma de Barcelona, E-08193 Bellaterra, Spain

Received: 16 January 2005 /
Published online: 29 June 2005 –

Abstract. This manuscript reviews recent applications of the nuclear shell-model for the calculation of several quantities relevant for the core-collapse supernova dynamics and nucleosynthesis. These include electron capture rates and neutrino-nucleus cross sections for inelastic scattering. It is shown that electron capture rates on nuclei dominates over capture on free protons during the collapse leading to significant changes in the hydrodynamics of core collapse and bounce. Neutrino-nucleus cross sections at supernova neutrino energies can be determined from precise data on the magnetic dipole strength. The results agree well with large-scale shell-model calculations, validating this model.

PACS. 21.60.Cs Shell model – 26.50.+x Nuclear physics aspects of novae, supernovae, and other explosive environments

1 Introduction

Stars with masses exceeding roughly 10 $M_\odot$ reach a moment in their evolution when their iron core provides no further source of nuclear energy generation. At this time, they collapse and, if not too massive, bounce and explode in spectacular events known as type II or Ib/c supernovae. These explosions mark the formation of a neutron star or black hole at the end of the life of the star and play a preeminent role in the nucleosynthesis and chemical evolution of the galaxy. The evolution in the core is determined by the competition of gravity, that produces the collapse of the core, and the weak interaction, that determines the rate at which electrons are captured and the rate at which neutrinos are trapped during the collapse.

The early phases, known as presupernova evolution, follow the late-stage stellar evolution until core densities just below $10^{10}\,\mathrm{g\,cm^{-3}}$ and temperatures between 5 and 10 GK are reached. Stellar evolution until this time requires the consideration of an extensive nuclear network, but is simplified by the fact that neutrinos need only be treated as a sink of energy and lepton number. This is no longer valid at later stages of the collapse: as the weak interaction rates increase with the increasing density, the neutrino mean free paths become shorter so that the neutrinos eventually proceed through all phases of free streaming, diffusion, and trapping. An adequate handling of the transitions between these transport regimes necessitates a detailed time- and space-dependent bookkeeping of the neutrino distributions in the core.

Advantageously, the temperature during the collapse and explosion are high enough that the matter composition is given by nuclear statistical equilibrium without the need of reaction networks for the strong and electromagnetic interactions. As the entropy is low during the collapse, the matter composition is dominated by the nuclei with the largest binding energy for a given Y_e (defined as the number of electrons per nucleon). In order to correctly determine the evolution of the system a reliable estimate of the different weak interaction rates on the nuclei present is necessary [1]. In the early phases of the collapse (presupernova evolution) the main weak interaction processes are electron/positron capture and $\beta^\pm$ decays. Later during the collapse neutrino matter interactions and in particular inelastic processes are also important. Of these neutrino-nucleus inelastic scattering is currently not considered in collapse simulations. The calculation of the different rates is a challenging problem in nuclear structure. Moreover, due to the large temperatures and densities present in the astrophysical environment their calculation presents some peculiarities that are discussed in the following sections.

2 Presupernova evolution

The main weak interaction processes during the final evolution of a massive star are electron capture and beta decays. Its determination requires the calculation of Fermi and Gamow-Teller (GT) transitions. While the treatment of Fermi transitions (important only for beta decays) is straightforward, a correct description of the GT transitions is a difficult problem in nuclear structure. In the astrophysical environment nuclei are fully ionized,

[a] Conference presenter; e-mail: martinez@ieec.uab.es

so electrons are captured from the degenerate electron plasma. The energies of the electrons are high enough to induce transitions to the Gamow-Teller resonance. Shortly after the discovery of this collective excitation Bethe *et al.* [2] recognized its importance for stellar electron capture. This process is mainly sensitive to the location, fragmentation and total strength of the Gamow-Teller resonance. The presence of a degenerate electron gas blocks the phase space for the produced electron in beta decay. Then, the decay rate of a given nuclear state is greatly reduced or even completely blocked at high densities. However, due to the finite temperature, excited states in the decaying nucleus can be thermally populated. Some of these states are connected by large GT transitions to low-lying states in the daughter nucleus, which with increased phase space can significantly contribute to the stellar beta decay rates. The importance of these states in the parent nucleus for the beta decay was first recognized by Fuller, Fowler and Newman (FFN) [3,4,5,6], who coined the term "backresonances".

Over the years many calculations of weak interaction rates for astrophysical applications have become available [7,8,9,10,11,12,13]. For approximately 15 years, though, the standard in the field were the tabulations of Fuller, Fowler and Newman [3,4,5,6]. These authors calculated rates for electron capture, positron capture, beta decay and positron emission plus the associated neutrino losses for all the astrophysical relevant nuclei ranging in mass number from 21 to 60. Their calculations were based upon an examination of all available experimental information in the mid 1980s for individual transitions between ground states and low-lying excited states in the nuclei of interest. Recognizing that this only saturated a small part of the Gamow-Teller distribution, they added the collective strength via a single-state representation whose position and strength was parametrized using an independent particle model.

Recent experimental data on GT distributions in iron group nuclei [14,15,16,17,18,19,20,21], measured in charge exchange reactions [22,23], show that the GT strength is strongly quenched (reduced), compared with the independent-particle-model value, and fragmented over many states in the daughter nucleus. Both effects are caused by the residual interaction among the valence nucleons. An accurate description of these correlations is essential for a reliable evaluation of the stellar weak-interaction rates due to the large dependence of the available phase-space on the electron energy, particularly for the stellar electron-capture rates [3,24]. The shell model is the only known tool to reliably describe GT distributions in nuclei [25]. Indeed, ref. [26] demonstrated that the shell model reproduces very well all measured GT_+ distributions (in this direction a proton is converted to a neutron, as in electron capture) for nuclei in the iron mass range and gives a very reasonable account of the experimentally known GT_- distributions (in this direction a neutron is converted to a proton, as in β decay). However, the limited experimental resolution ($\sim$ 1 MeV) achieved by the pioneering (n,p)-type charge-exchange experiments did not allow for a detailed determination of the fragmentation of the GT strength in individual states. Very recently, high-resolution GT_+ distributions measured at KVI, via the $(d,{}^2\mathrm{He})$ reaction, have become available for two iron group nuclei, ^{51}V [27] and ^{58}Ni [28]. The experimental data for ^{51}V are compared in fig. 1 with a shell-model calculation using the KB3G interaction [29].

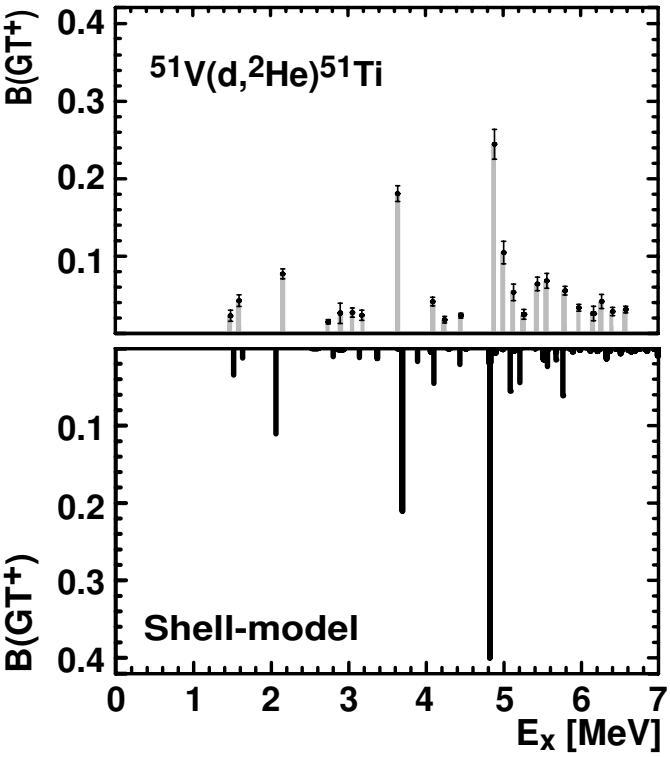

Fig. 1. Comparison of the shell-model GT_+ distribution (lower panel) for ^{51}V with the high resolution $(d,{}^2\mathrm{He})$ data [27]. The shell-model distribution includes a quenching factor of $(0.74)^2$.

Several years ago, it was pointed out that the interacting shell model is the method of choice for the calculation of stellar weak-interaction rates [13,30,31,32,33]. Following the work of ref. [25], shell-model rates for all the relevant weak processes for *sd*-shell nuclei (A = 17–39) were calculated in ref. [34]. This work was then extended to heavier nuclei (A = 45–65) based on shell-model calculations in the complete pf-shell [24,35]. Following the spirit of FFN, the shell model results have been replaced by experimental data (energy positions, transition strengths) wherever available.

Reference [24] compares the shell-model–based rates with the ones computed by FFN. The shell-model rates are nearly always smaller than the FFN ones at the relevant temperatures and densities. The differences are caused by a reduction of the Gamow-Teller strength (quenching) compared to the independent-particle-model value and a systematic misplacement of the Gamow-Teller centroid (mean energy value of the Gamow-Teller distribution) in nuclei depending on the pairing structure. In some cases, experimental data that were not available to Fuller, Fowler and Newman, but could be used now, led to significant changes.

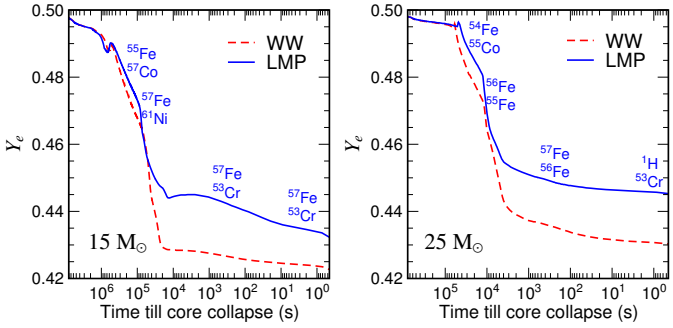

Fig. 2. Evolution of the Y_e value in the center of a 15 $M_\odot$ star (left panel) and a 25 $M_\odot$ star (right panel) as a function of time until bounce. The dashed line shows the evolution in the Woosley and Weaver models (WW) [36], that use the FFN rates, while the solid line shows the results using the shell-model–based weak-interaction rates of Langanke and Martínez-Pinedo (LMP). The most important nuclei in the determination of the electron-capture rate for the calculations adopting the shell-model rates are indicated at different times.

To understand the effect of these differences it is illustrative to investigate the role of the weak-interaction rates in greater detail. The evolution of Y_e during the presupernova phase is plotted in fig. 2. Weak processes become particularly important in reducing Y_e below 0.5 after oxygen depletion ($\sim 10^7$ s and 10^6 s before core collapse for the 15 $M_\odot$ and 25 $M_\odot$ stars, respectively) and Y_e begins a decline which becomes precipitous during silicon burning. Initially electron capture occurs much more rapidly than beta decay. As the shell-model rates are generally smaller than the FFN electron capture rates, the initial reduction of Y_e is smaller in the new models; the temperature in these models is correspondingly larger as less energy is radiated away by neutrino emission.

An important feature of the new models is shown in the left panel of fig. 2. For times between 10^4 and 10^3 s before core collapse, Y_e increases due to the fact that beta decay becomes temporarily competitive with electron capture after silicon depletion in the core and during silicon shell burning. This had been foreseen in ref. [37]. The presence of an important beta decay contribution has two effects. Obviously it counteracts the reduction of Y_e in the core, but equally important, beta decays are an additional neutrino source and thus they add to the cooling of the core and a reduction in entropy. This cooling can be quite efficient as often the average neutrino energy in the involved beta decays is larger than for the competing electron captures. As a consequence the new models have significantly lower core temperatures than the WW models after silicon burning. At later stages of the collapse, beta decay becomes unimportant again as an increased electron chemical potential drastically reduces the phase space.

We note that the shell model weak interaction rates predict the presupernova evolution to proceed along a temperature-density-Y_e trajectory where the weak processes are dominated by nuclei rather close to stability. Thus it will be possible, after next generation radioactive ion-beam facilities become operational, to further constrain the shell-model calculations by measuring relevant GT distributions for unstable nuclei by charge-exchange reaction, where we emphasize that the GT$_+$ distribution is also crucial for stellar β-decays [31]. Figure 2 identifies those nuclei which dominate (defined by the product of abundance times rate) the electron capture during various stages of the final evolution of 15 $M_\odot$ and 25 $M_\odot$ stars. An exhaustive list of the most important nuclei for both electron capture and beta decay during the final stages of stellar evolution for stars of different masses is given in ref. [38].

3 Electron capture during the collapse

Calculations of the reaction rate for electron capture in the collapsing core requires two components: the appropriate electron capture reaction rates and the knowledge of the nuclear composition. The coupling of electron capture rates to energy-dependent neutrino transport adds an additional requirement: information about the spectra of emitted neutrinos. These spectra can be parametrized using the prescription of ref. [39]. During the collapse most of the collapsing matter survives in heavy nuclei as the entropy is rather low [2]. Y_e decreases during the collapse due to electron capture, making the matter composition more neutron rich and hence favoring increasingly heavy nuclei. Unlike in stellar evolution and supernova nucleosynthesis simulations, where the nuclear composition is tracked in detail via a reaction network [40,41], the composition used in supernova simulations is calculated by the equation of state, which assumes nuclear statistical equilibrium (NSE). Typically, the information about the nuclear composition provided by the equation of state is limited to the mass fractions of free neutrons and protons, α particles and the sum of all heavy nuclei, as well as the identity of an average heavy nucleus, calculated either in the liquid drop framework [42] or based on a relativistic mean field model [43,44]. It should be noted that the most abundant nucleus is not necessarily the nucleus which dominate electron capture during the infall phase. For the evaluation of reaction rates on nuclei, due to the dependence on nuclear structure effects, a single nucleus approximation is not sufficient. It must be replaced by an ensemble average.

Traditionally, in collapse simulations the treatment of electron capture on nuclei is schematic and rather simplistic. The nuclear structure required to derive the capture rate is then described solely on the basis of an independent-particle model for iron-range nuclei, *i.e.*, considering only Gamow-Teller transitions from $f_{7/2}$ protons to $f_{5/2}$ neutrons [2,45,46,47]. In particular, this model predicts that electron capture vanishes for nuclei with neutron number $N \geq 40$, arguing that Gamow-Teller transitions are blocked due to the Pauli principle, as all possible final neutron orbitals are already occupied in nuclei with $N \geq 40$ [48]. These nuclei dominate the composition for densities larger than a few 10^{10} g cm^3. As a consequence of the model applied in previous collapse simulations, electron capture on nuclei ceases at these densities and the capture is entirely due to free protons. It has been

pointed out [49] that this picture is too simple and that the blocking of the Gamow-Teller transitions will be overcome by thermal excitations which either moves protons into the $g_{9/2}$ orbit or removes neutrons from the pf-shell, in both ways unblocking the GT transitions. According to the work of ref. [49], due to "thermal unblocking" GT transitions dominate again for temperatures of the order of 1.5 MeV. A more important unblocking effect, which is already relevant at lower temperatures is expected from the residual interaction which will mix the $g_{9/2}$ and higher orbitals with the pf shell [50,51].

The calculation of electron capture on nuclei during the collapse phase requires a model that is able to describe the correlations and at the same time the high density of levels that can be thermally populated at moderate excitation energies. Direct shell-model diagonalizations are not yet possible due to the large model spaces involved. The calculations can be done using the Shell Model Monte Carlo approach [52] which allows for the calculation of nuclear properties at finite temperature in unprecedentedly large model spaces. This model complemented with Random Phase Approximation calculations for the computation of the transitions necessary for the determination of the electron capture rate has been used recently for the calculation of the relevant rates for nuclei in the mass range $A = 65$–112 [51].

Figure 3 compares the electron capture rates for free protons and selected nuclei along a stellar trajectory taken from [53]. These nuclei are abundant at different stages of the collapse. For all the nuclei, the rates are dominated by GT transitions at low densities, while forbidden transitions contribute sizably for $\rho \gtrsim 10^{11}\,\mathrm{g\,cm^{-3}}$. The electron chemical potential μ_e and the reaction Q value are the two important energy scales of the capture process. For the lowest densities the electron chemical potential ($\mu_e \approx 6\,\mathrm{MeV}$ for $\rho = 5 \times 10^9\,\mathrm{g\,cm^{-3}}$) is of the same order than the typical nuclear Q-value. Then, the electron capture rates on nuclei are very sensitive to the Q-value and smaller than the rate on protons. For higher densities the chemical potential grows much faster than the Q-value and the rate becomes independent of the heavy nucleus. Due to the much smaller Q-value, the electron capture rate on free protons is larger than the rates on the abundant nuclei during the collapse. However, this is misleading as the low entropy keeps the protons significantly less abundant than heavy nuclei during the collapse. As the commonly used equations of state [42,43,44] do not provide any detailed information for the abundances of heavy nuclei, a Saha-like NSE was used for the calculation of the abundances in refs. [51,54]. Once the abundances are considered the reaction rate for electron capture on heavy nuclei ($R_h = \sum_i Y_i \lambda_i$, where the sum runs over all the nuclei present and Y_i denotes the number abundance of species i) dominates over the one of protons ($R_p = Y_p \lambda_p$) by roughly an order of magnitude throughout the collapse (lower panel, fig. 3) [51,54].

The main consequences of the improved treatment of electron capture rates on nuclei for the collapse have been explored in self-consistent one-dimensional neutrino radiation hydrodynamics by the Oak Ridge and Garching collaborations [54,55]. With the improved treatment of electron capture rate on heavy nuclei the total electron capture rate (heavy nuclei plus protons) is larger than previously assumed resulting in a smaller value of Y_e. This translates into a smaller size of the homologous core (proportional to Y_e^2) so that the shock wave, which is generated at the edge of the homologous core, has to traverse more material in the new models which appears to make successful explosions more difficult. However, the reduction in capture rates for lighter nuclei ($A = 45$–65, see sect. 2), which are abundant further out in the core alters the core profile as well and in fact makes the shock wave travel to slightly larger radii in the new supernova models [54]. Nevertheless, the new one-dimensional models do not explode. However, the changes in entropy and lepton gradients may significantly alter the location, extent and strength of the proto-neutron star convection [54,56]. Figure 4 shows the typical differences between the old supernova simulations (without capture on nuclei) and the new ones for the velocity and Y_e core profiles at the moment of shock formation.

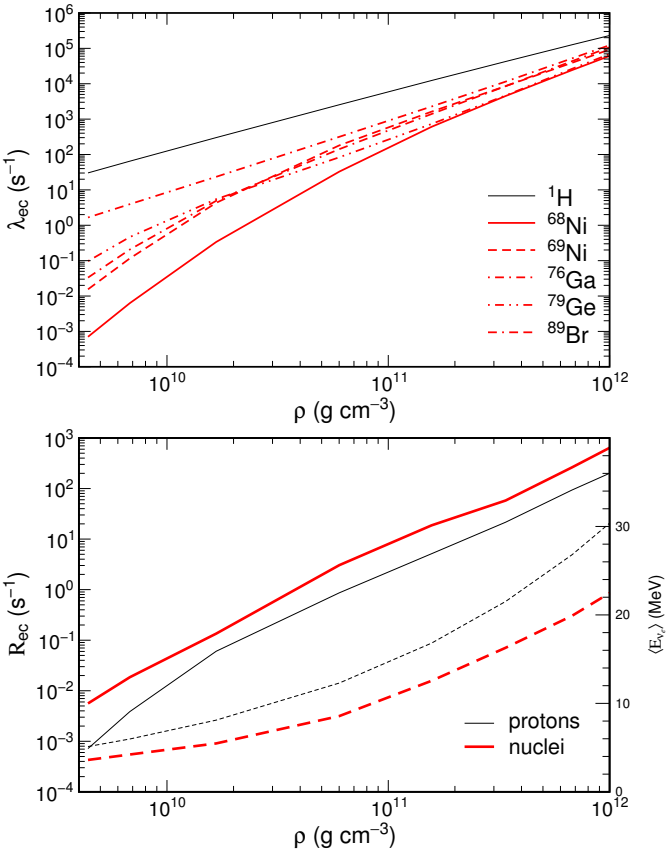

Fig. 3. Upper panel: comparison of the electron capture rates on free protons and selected nuclei as function of density along a stellar collapse trajectory taken from [53]. Lower panel: the reaction rates (abundance times rate) for electron capture on protons (thin line) and nuclei (thick line) are compared as a function of density along the same stellar collapse trajectory. The dashed lines (right scale) show the related average energy of the neutrinos emitted by capture on nuclei and protons.

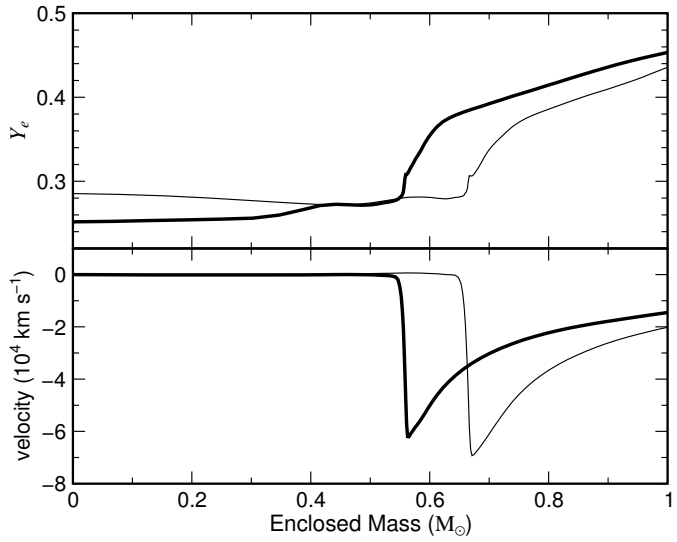

Fig. 4. The electron fraction an velocity as a function of the enclosed mass at bounce for a 15 $M_\odot$ model [57]. The thin line is a simulation using the Bruenn parametrization [45,46,47], which neglects electron capture rates on nuclei with neutron number $N > 40$.

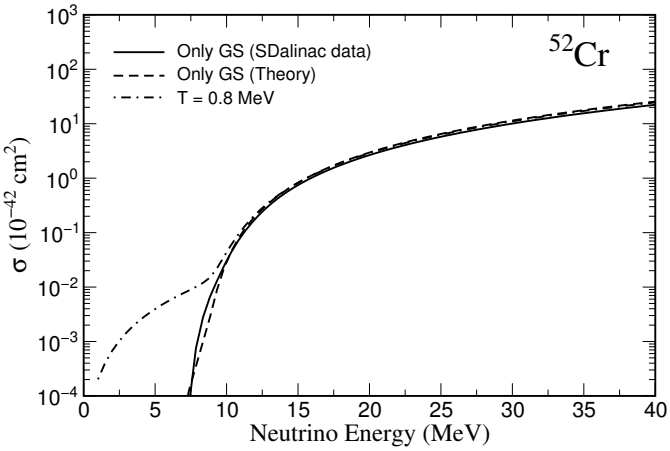

Fig. 5. Neutrino-nucleus cross sections calculated from the $M1$ data (solid lines) and the shell-model GT_0 distributions (dashed). The dot-dashed line shows the cross section once finite temperature effects are included.

4 Neutrinos in supernova

Neutrinos play an important role in core-collapse supernova dynamics and nucleosynthesis. During the collapse the interaction of neutrinos with matter (mainly elastic scattering with nuclei) leads to neutrino trapping. Once the neutrinos are trapped, they achieve thermal equilibrium with matter via inelastic processes. One process so far neglected in simulations but that can be relevant for the thermalization during infall [58] is inelastic neutral-current neutrino-nucleus scattering. Neutrino-nucleus cross sections are also important for the r-process nucleosynthesis and in the synthesis of certain elements such as ^{11}B and ^{19}F and ^{138}La by the so-called ν-process [59]. As the ν-process involves both neutral-current and charge-current reactions it can provide quite useful constrains for the supernova spectra of ν_e and ν_μ, ν_τ neutrinos [60].

Currently no data for inelastic neutrino-nucleus scattering are available (except for the ground state transition to the $T = 1$ state at 15.11 MeV in ^{12}C). A dedicated detector at the Oak Ridge spallation neutron source has been proposed to measure some neutrino-nucleus cross sections relevant for core-collapse supernova (mainly in the iron mass range) [61]. To sharpen the experimental program at this facility and to improve supernova simulations, inelastic neutrino-nucleus cross sections should be incorporated into the supernova models. Based in shell-model (for the GT transitions) and RPA calculations (for the forbidden transitions) we have recently calculated the required cross sections for around 50 nuclei in the iron mass range [62]. The theoretical calculations can be constrained by precise $M1$ data, obtained by inelastic electron scattering, as they supply the required information about the GT_0 distribution which determines the inelastic neutrino-nucleus cross sections for supernova neutrino energies [63]. The reason is that for $M1$ transitions the isovector part dominates and the spin part of the isovector $M1$ operator is proportional to the spin part of the GT_0 operator. Thus, experimental $M1$ data provides the needed GT_0 information to determine supernova neutrino-nucleus cross sections provided that the isoscalar and orbital pieces present in the $M1$ operator can be neglected or removed. This can be easily done as the orbital and spin $M1$ responses are well separated energetically and moreover the orbital part is strongly related to deformation and suppressed in spherical nuclei, like ^{50}Ti, ^{52}Cr and ^{54}Fe. These nuclei have the additional advantage that $M1$ data exist from high-resolution inelastic electron scattering experiments [64]. We have carried out shell-model calculations for the GT_0 and various components of the $M1$ response in these nuclei. The shell-model calculations reproduce the data rather well [63]. Figure 5 compares the inelastic neutrino-nucleus cross section for ^{52}Cr (results for the other two nuclei are available on [63]) computed from the $M1$ data and the shell-model calculations. This comparison validates the shell-model as a tool for the calculation of the relevant supernova neutrino-nucleus cross sections. This model can then be used for the calculation of the cross sections at the finite temperature in the astrophysical environment. The main effect of finite temperature is an enhancement of cross sections for low energy neutrinos [63,65].

This work is partly supported by the Spanish MEC and the European Union ERDF under contracts AYA2002-04094-C03-02 and AYA2003-06128. It is a pleasure to thank our collaborators D.J. Dean, W.R. Hix, H.Th. Janka, A. Juodagalvis, K. Langanke, M. Liebendörfer, O.E.B. Messer, A. Mezzacappa, P. von Neumann-Cosel, A. Richter, J. Sampaio.

References

1. K. Langanke, G. Martínez-Pinedo, Rev. Mod. Phys. **75**, 819 (2003).
2. H.A. Bethe, G.E. Brown, J. Applegate, J.M. Lattimer, Nucl. Phys. A **324**, 487 (1979).
3. G.M. Fuller, W.A. Fowler, M.J. Newman, Astrophys. J. Suppl. **42**, 447 (1980).
4. G.M. Fuller, W.A. Fowler, M.J. Newman, Astrophys. J. **252**, 715 (1982).
5. G.M. Fuller, W.A. Fowler, M.J. Newman, Astrophys. J. Suppl. **48**, 279 (1982).
6. G.M. Fuller, W.A. Fowler, M.J. Newman, Astrophys. J. **293**, 1 (1985).
7. C.J. Hansen, PhD Thesis, Yale University (1966).
8. C.J. Hansen, Astrophys. Space Sci. **1**, 499 (1968).
9. T. Mazurek, PhD Thesis, Yeshiva University (1973).
10. T. Mazurek, J.W. Truran, A.G.W. Cameron, Astrophys. Space Sci. **27**, 161 (1974).
11. K. Takahashi, M. Yamada, T. Kondoh, At. Data. Nucl. Data Tables **12**, 101 (1973).
12. K. Takahashi, M.F. El Eid, W. Hillebrandt, Astron. Astrophys. **67**, 185 (1978).
13. M.B. Aufderheide, I. Fushiki, S.E. Woosley, D.H. Hartmann, Astrophys. J. Suppl. **91**, 389 (1994).
14. A.L. Williams *et al.*, Phys. Rev. C **51**, 1144 (1995).
15. S. El-Kateb *et al.*, Phys. Rev. C **49**, 3128 (1994).
16. W.P. Alford, *et al.*, Phys. Rev. C **48**, 2818 (1993).
17. W.P. Alford *et al.*, Nucl. Phys. A **514**, 49 (1990).
18. M.C. Vetterli *et al.*, Phys. Rev. C **40**, 559 (1990).
19. J. Rapaport *et al.*, Nucl. Phys. A **410**, 371 (1983).
20. B.D. Anderson, C. Lebo, A.R. Baldwin, T. Chittrakarn, R. Madey, J.W. Watson, Phys. Rev. C **41**, 1474 (1990).
21. B.D. Anderson *et al.*, Phys. Rev. C **31**, 1161 (1985).
22. C.D. Goodman *et al.*, Phys. Rev. Lett. **44**, 1755 (1980).
23. F. Osterfeld, Rev. Mod. Phys. **64**, 491 (1992).
24. K. Langanke, G. Martínez-Pinedo, Nucl. Phys. A **673**, 481 (2000).
25. B.A. Brown, B.H. Wildenthal, Annu. Rev. Nucl. Part. Sci. **38**, 29 (1988).
26. E. Caurier, K. Langanke, G. Martínez-Pinedo, F. Nowacki, Nucl. Phys. A **653**, 439 (1999).
27. C. Bäumer *et al.*, Phys. Rev. C **68**, 031303 (2003).
28. M. Hagemann *et al.*, Phys. Lett. B **579**, 251 (2004).
29. A. Poves, J. Sánchez-Solano, E. Caurier, F. Nowacki, Nucl. Phys. A **694**, 157 (2001).
30. M.B. Aufderheide, Nucl. Phys. A **526**, 161 (1991).
31. M.B. Aufderheide, S.D. Bloom, G.J. Mathews, D.A. Resler, Phys. Rev. C **53**, 3139 (1996).
32. M.B. Aufderheide, S.D. Bloom, D.A. Ressler, G.J. Mathews, Phys. Rev. C **47**, 2961 (1993).
33. M.B. Aufderheide, S.D. Bloom, D.A. Ressler, G.J. Mathews, Phys. Rev. C **48**, 1677 (1993).
34. T. Oda, M. Hino, K. Muto, M. Takahara, K. Sato, At. Data Nucl. Data Tables **56**, 231 (1994).
35. K. Langanke, G. Martínez-Pinedo, At. Data. Nucl. Data Tables **79**, 1 (2001).
36. S.E. Woosley, T.A. Weaver, Astrophys. J. Suppl. **101**, 181 (1995).
37. M.B. Aufderheide, I. Fushiki, G.M. Fuller, T.A. Weaver, Astrophys. J. **424**, 257 (1994).
38. A. Heger, S.E. Woosley, G. Martínez-Pinedo, K. Langanke, Astrophys. J. **560**, 307 (2001).
39. K. Langanke, G. Martínez-Pinedo, J.M. Sampaio, Phys. Rev. C **64**, 055801 (2001).
40. S.E. Woosley, in *Nucleosynthesis and Chemical Evolution*, edited by B. Hauck, A. Maeder, G. Meynet, Vol. **16** of *Saas-Fee Advanced Courses* (Geneva Observatory, 1986) pp. 1-195.
41. W.R. Hix, F.-K. Thielemann, Astrophys. J. **511**, 862 (1999).
42. J.M. Lattimer, F.D. Swesty, Nucl. Phys. A **535**, 331 (1991).
43. H. Shen, H. Toki, K. Oyamatsu, K. Sumiyoshi, Nucl. Phys. A **637**, 435 (1998).
44. H. Shen, H. Toki, K. Oyamatsu, K. Sumiyoshi, Prog. Theor. Phys. **100**, 1013 (1998).
45. S.W. Bruenn, Astrophys. J. Suppl. **58**, 771 (1985).
46. A. Mezzacappa, S.W. Bruenn, Astrophys. J. **405**, 637 (1993).
47. A. Mezzacappa, S.W. Bruenn, Astrophys. J. **410**, 740 (1993).
48. G.M. Fuller, Astrophys. J. **252**, 741 (1982).
49. J. Cooperstein, J. Wambach, Nucl. Phys. A **420**, 591 (1984).
50. K. Langanke, E. Kolbe, D.J. Dean, Phys. Rev. C **63**, 032801 (2001).
51. K. Langanke *et al.*, Phys. Rev. Lett. **90**, 241102 (2003).
52. S.E. Koonin, D.J. Dean, K. Langanke, Phys. Rep. **278**, 2 (1997).
53. A. Mezzacappa, M. Liebendörfer, O.E. Bronson Messer, W. Raphael Hix, F.-K. Thielemann, S.W. Bruenn, Phys. Rev. Lett. **86**, 1935 (2001).
54. W.R. Hix *et al.*, Phys. Rev. Lett. **91**, 201102 (2003).
55. M. Rampp, H.-T. Janka, private communication.
56. G. Martínez-Pinedo, M. Liebendörfer, D. Frekers, submitted to Nucl. Phys. A (2004), astro-ph/0412091.
57. A. Heger, K. Langanke, G. Martínez-Pinedo, S.E. Woosley, Phys. Rev. Lett. **86**, 1678 (2001).
58. S.W. Bruenn, W.C. Haxton, Astrophys. J. **376**, 678 (1991).
59. S.E. Woosley, D.H. Hartmann, R.D. Hoffman, W.C. Haxton, Astrophys. J. **356**, 272 (1990).
60. A. Heger, E. Kolbe, W. Haxton, K. Langanke, G. Martínez-Pinedo, S.E. Woosley, Phys. Lett. B **606**, 258 (2005).
61. F.T. Avignone, L. Chatterjee, Y.V. Efremenko, M. Strayer (Editors), *Neutrino physics at spallation neutron sources*, J. Phys. G **29**, 2497 (2003).
62. A. Juodagalvis, K. Langanke, G. Martínez-Pinedo, W.R. Hix, D.J. Dean, J.M. Sampaio, Nucl. Phys. A **747**, 87 (2005).
63. K. Langanke, G. Martínez-Pinedo, P. von Neumann-Cosel, A. Richter, Phys. Rev. Lett. **93**, 202501 (2004).
64. P. von Neumann-Cosel, A. Poves, J. Retamosa, A. Richter, Phys. Lett. B **443**, 1 (1998).
65. J.M. Sampaio, K. Langanke, G. Martínez-Pinedo, D.J. Dean, Phys. Lett. B **529**, 19 (2002).